The Odijk Regime in Slits

Douglas R. Tree, Wesley F. Reinhart, and Kevin D. Dorfman*

Department of Chemical Engineering and Materials Science, University of Minnesota, Minneapolis, Minnesota 55455, United States

E-mail: dorfman@umn.edu

Abstract

De Gennes' blob theory has been remarkably successful at describing weakly confined polymers in both slits and channels, and comparable results surround Odijk's theory of deflection segments for strongly confined wormlike polymers in nanochannels. However, given the success of Odijk's theory in channels, it is remarkable that there is no comprehensive theory for the simple case of a wormlike polymer strongly confined between two parallel plates. We propose such a theory by drawing inspiration from the existing literature on ideal wormlike chains in slits and Daoud and de Gennes' idea of mapping a slit-confined chain to a two-dimensional chain. We postulate that the chain can be quantitatively described as a two-dimensional wormlike chain with a weak perturbation in the confining dimension due to deflection segments. By incorporating the effects of real chains, where the variable slit depth adds additional subtlety due to concomitant changes in the strength of excluded volume interactions, our theory predicts the existence of three distinct subregimes. We investigate the validity of our claims by performing Monte Carlo simulations of a slit-confined wormlike chain using an off-lattice implementation of the pruned-enriched Rosenbluth method. From these simulations, we find strong numerical evidence supporting our predictions, including the existence of subregimes within the Odijk regime.

*To whom correspondence should be addressed

1 Introduction

The subject of confined wormlike polymers has garnered recent attention due to the confluence of fundamental questions in polymer physics and the demand for new genomic analysis tools.[1,2] One of the simplest modes of confinement, both theoretically and experimentally, involves placing a wormlike chain between two parallel planes. This type of confinement exhibits a rich set of equilibrium behavior due to the interplay between confinement, chain stiffness, excluded volume interactions and chain length.[3–10] However, despite the apparently simple geometry, details surrounding strongly confined wormlike polymers in slits remain remarkably controversial.[7–9] In this article, we attempt to resolve the issue by proposing a comprehensive theory of the Odijk regime in slits, which we subsequently support with Monte Carlo simulations.

The source of disagreement in the literature surrounds a divergence of approach in attempting to resolve the details of the Odijk regime in slits. Using a combination of field theory and simulation, Burkhardt *et al.*[11–13] and Chen and Sullivan[14] have examined polymers absent any intra-chain interactions (*i.e.* ideal chains). By different methods, both groups[11–14] produce strong, independent evidence for the existence of deflection segments in slits, and Burkhardt *et al.*[11–13] provide precise predictions of the relevant numerical prefactors. Alternatively, Doyle *et al.*[7,9] and Cifra[8] have studied real chain models, which include excluded volume interactions and aim to directly compare with experiments using DNA. In the latter work, the evidence for the Odijk regime is less clear — so much so that one study suggests that the Odijk regime may not even exist in slit confinement.[8]

We reconcile these threads in the literature with a theory for strongly confined polymers in slits based on the two simple postulates that are embodied in the schematic shown in Figure 1. We first posit that a sufficiently long, strongly-confined chain may be viewed as a two-dimensional chain with weak swelling in the direction normal to the confinement plane due to deflection segments, as seen in the left panel in Figure 1. Such a theory is plausible if the formation of deflection segments is (i) independent of chain properties such as persistence length and excluded volume and (ii) separable from the behavior of the chain along the other dimensions. The fact that the chain is essentially two-dimensional should not be particularly surprising, since it is analogous to

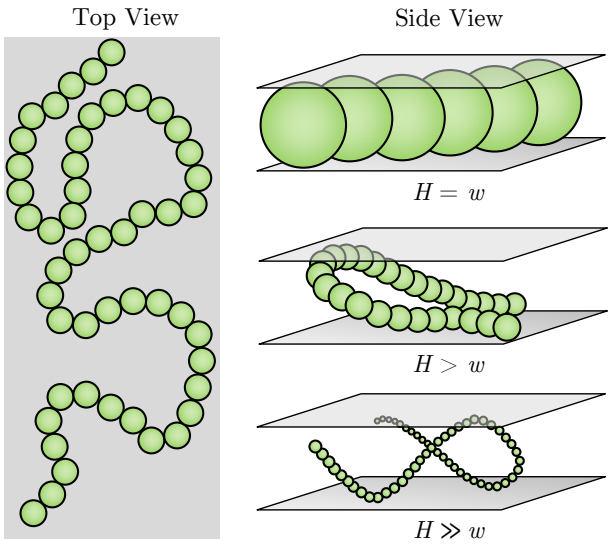

Figure 1: Schematic representation of real chains in varying degrees of strong, uniaxial confinement (i.e. $H \ll l_p$). The left presents a top-down view, showing a two-dimensional wormlike chain composed of deflection segments. The right shows a cross-sectional view, which highlights the effect of excluded volume strength. For $H = w$, the polymer becomes a wormlike chain confined to a plane and is a purely, two-dimensional self-avoiding walk. Alternatively, when $H \gg w$ the probability of segment interactions is greatly suppressed and the chain becomes ideal. Note that this schematic does not depict a fixed value of the persistence length, which must be much greater than the slit height in all cases.

the mapping proposed by Daoud and de Gennes [15] for blob regimes in weak confinement. Indeed, this analogy is easily visualized if one imagines that the beads of the chain in the left panel of Figure 1 are replaced by blobs.

The second postulate concerns the nature of chains with excluded volume and is shown in the right panel of Figure 1. When the slight height, H, is much greater than the chain width, w, the probability of intra-chain interactions becomes vanishingly small and the ideal limit is recovered. The opposite happens when $H = w$. Here, the chain cannot avoid itself and becomes equivalent to a purely two-dimensional, self-avoiding wormlike chain in the plane of confinement. [16,17] The case $H > w$ exhibits some probability of interaction and is thus a more complicated, intermediate state. Using these insights, we propose that a theory that aims to describe slit-confined chains with excluded volume must be consistent with the ideal chain case discussed in the previous paragraph when $H \gg w$ and must also reduce to a real, two-dimensional wormlike chain when $H = w$.

We proceed to incorporate these postulates into a theory of the Odijk regime in slits. First, we extend the ideal chain results of Burkhardt *et al.*[11–13] and Chen and Sullivan[14] into a theory that quantitatively relates a strongly confined chain and a 2D wormlike chain. We then incorporate the effects of excluded volume using a Flory theory originally proposed by Odijk,[6] which accounts for both the limits $H \gg w$ and $H = w$ described in Figure 1. Having reviewed and expanded on the theory of the Odijk regime in slits, we compare its predictions to numerical results of a discrete wormlike chain model using an off-lattice version of the pruned-enriched Rosenbluth method.[18] The method allows us to explore a large region of the applicable parameter space over which we find excellent agreement with our theory. Finally, we conclude with a brief discussion of some of the implications of our findings.

2 Theoretical Results

2.1 Ideal Chains

We now consider detailed theoretical results for the equilibrium behavior of an ideal wormlike chain in the Odijk regime in slits. Alongside our own results, we also review prior work on ideal chains, which is necessary for a self-contained discussion of chains with excluded volume in Section 2.2. Given the need to review this material and our desire to preserve logical continuity, ideas and equations attributable to other authors are often simply distinguished with a citation. Conversely, an equation with no such citation can be considered an original contribution.

A slit-confined, ideal wormlike chain has three length scales which characterize its behavior: a slit height, H, a contour length L and a persistence length l_p. In the present work, we will focus solely on the region of the parameter space where $H \ll l_p$, which we take as the definition of the Odijk regime. Furthermore, we restrict our scope to proper uniaxial confinement, with an infinite domain extending in the directions tangent to the floor and ceiling of the slit. In practice slits must of course have side walls, but it is anticipated that the walls are unimportant for the equilibrium conformation as long as the polymer size, R, is small compared to the distance between

the walls.[6,19]

The Odijk regime is distinguished by the emergence of a new length scale, which manifests itself when $H \ll l_p$.[20] This length scale, called the deflection length[20]

$$\lambda = H^{2/3} l_p^{1/3} \tag{1}$$

describes the contour length of the confined chain between intermittent collisions with the top and bottom of the slit walls (see Figure 1). Since the persistence length is large on the scale of confinement, bending of the chain is minimal between such deflections, and a segment of the chain of the size of the deflection length is essentially rod-like.

In addition to the restriction that H be much less than l_p, the contour length of the chain must be sufficiently long to enter the Odijk regime. In fact, given that $H \ll l_p$ we can distinguish between three regimes of behavior based upon the contour length of the chain. When $L \gg \lambda$ we achieve the Odijk regime, where we have sufficient chain length to exhibit a large number of deflection segments. On the other hand, if $L \ll H$ the chain is weakly confined and behaves similar to rod-like particle in the bulk. Due to the separation of length scales between H and λ when l_p is large, there is an intermediate regime which arises when $H \ll L \ll \lambda$. This regime is characterized by orientational ordering of the stiff chain, similar to nematic ordering of rod-like liquid crystals.[21]

The transition from bulk behavior to the Odijk regime can be characterized by both a projection of the contour length onto the plane of confinement, $L_\parallel$, as well as a confinement free energy, ΔF_c. We define the projected contour length as the length of the chain contour projected onto the plane parallel to the slit surface

$$L_\parallel = \left\langle \int_0^L \left| \frac{\partial \mathbf{r}_\parallel}{\partial s} \right| ds \right\rangle \tag{2}$$

where $\mathbf{r}_\parallel(s) = \mathbf{e}_\perp \times \mathbf{r}(s) \times \mathbf{e}_\perp$ is the projection of the contour of the chain, $\mathbf{r}(s)$, onto the slit surface assuming that $\mathbf{e}_\perp$ is a unit normal to the plane of confinement. The confinement free energy is given by

$$\Delta F_c = k_B T \ln \frac{Z}{Z_0} \tag{3}$$

where Z is the configurational partition function, Z_0 is the partition function for an ideal, unconfined wormlike chain, k_B is Boltzmann's constant and T is the absolute temperature.

Focusing on the projected contour length for the moment, we note that it is difficult to obtain an analytical expression from Eq. 2, and we are forced to rely on numerical techniques. Fortunately some simple trigonometric arguments are sufficient to obtain approximate expressions for $L_\parallel$ in each regime. When $L \ll H$, the polymer is rod-like, and we can approximate the projected contour length as

$$L_\parallel \approx L\langle \cos\theta \rangle \tag{4}$$

where θ is the smaller angle between L and $L_\parallel$. Because L is smaller than the slit height, the rod is free to rotate isotropically, giving[21]

$$L_\parallel = \frac{\pi L}{4} \tag{5}$$

which is what we would expect as bulk-like behavior. In the orientation regime, when $H \ll L \ll \lambda$, the chain is still rod-like but can no longer rotate freely. In this case we can assume that $\theta \approx H/L$ is small and we can expand the right hand side of Eq. 4 to give[20]

$$L_\parallel \approx L\left[1 - \frac{1}{2}\left(\frac{H}{L}\right)^2\right] \tag{6}$$

A more careful evaluation of Eq. 2 yields only a change to the prefactor[11–13]

$$L_\parallel = L\left[1 - \alpha_L\left(\frac{H}{L}\right)^2\right] \tag{7}$$

with $\alpha_L = 0.09137$. Finally, in the Odijk regime, $L \gg \lambda$ and the chain consists of $N_\lambda = L/\lambda$ deflection segments. Assuming each deflection segment contributes a portion similar to the orientation regime, we substitute $L = \lambda$ into the right-hand side of Eq. 7 and multiply by N_λ to obtain[11–13,20]

$$L_\parallel = L\left[1 - \alpha_L\left(\frac{H}{l_p}\right)^{2/3}\right] \tag{8}$$

The confinement free energy also shows distinctive behavior in each of the three regimes. When $L \ll H$, a combination of a loss of translational and rotational entropy gives rise to[22,23]

$$\Delta F_c = -\ln\left(1 - \frac{L}{2H}\right) \tag{9}$$

This free energy is identical to that of a weakly confined polymer in larger slits ($H \gg l_p$) and is exactly half that of a weakly confined polymer in a square channel.[22,24] When $H \ll L \ll \lambda$, the loss of rotational entropy becomes more severe and[21,23]

$$\Delta F_c = k_B T \ln\left(\frac{2L}{H}\right) \tag{10}$$

When $L \gg \lambda$, dimensional analysis suggests that the confinement free energy ΔF is O($k_B T$) per deflection segment is[20,21,25]

$$\Delta F_c \sim k_B T \frac{L}{\lambda} \tag{11}$$

Odijk has pointed out that Eq. 11 is not equivalent to N_λ independent segments with a free energy given by Eq. 10.[20,21] Instead, Eq. 11 also accounts for the correlation between successive deflection segments due to chain connectivity.[21] Rearranging Eq. 11 and introducing a dimensionless confinement free energy per persistence length $\mathscr{F}$, gives[11–13,25]

$$\mathscr{F} \equiv \frac{\Delta F_c}{k_B T}\frac{l_p}{L} = A\frac{l_p}{\lambda} \tag{12}$$

where $A = 1.1036$ is a geometry-dependent prefactor previously calculated by Burkhardt *et al.*[11–13]

It is worth pointing out that since the Odijk regime is asymptotically approached when $H \ll l_p$, the confinement free energy smoothly varies between the strong confinement limit[20] and the weak confinement limit[15,26] as a function of H/l_p. Accordingly, Chen and Sullivan provide an

interpolation formula for the free energy of ideal chains as a function of slit height,[14]

$$\mathscr{F} = \frac{\pi^2/3\,(l_p/H)^2}{\left[5.146(l_p/H)^2 + 1.984(l_p/H) + 1\right]^{2/3}} \tag{13}$$

valid at all values of H/l_p. Note that Eq. 13 reduces to Eq. 12 in the limit $H/l_p \ll 1$.

In many experimental systems, $L \gg \lambda$ and the chain is long enough to be safely considered in the Odijk regime. In such systems (*e.g.* fluorescence microscopy experiments involving double-stranded DNA), the polymer size projected onto the confinement plane, $R_{\parallel}$, is directly observed. For our purposes it is more convenient to deal with the root-mean-square end-to-end distance

$$R \equiv \langle |\mathbf{r}(L) - \mathbf{r}(0)|^2 \rangle^{1/2} \tag{14}$$

Using simple trigonometric arguments similar to those above, $R_{\parallel}$ can be related to R by

$$R_{\parallel} = R\left[1 - \gamma\left(\frac{H}{R}\right)^2\right] \tag{15}$$

where γ is some unknown constant. Importantly, the ratio $R_{\parallel}/R$ given by Eq. 15 approaches one with increasing chain length regardless of the slit height, unlike $L_{\parallel}/L$, which remains a function of H/l_p. Therefore, because $R \gg \lambda \gg H$ is a requirement for the Odijk regime, one may safely assume that for most practical purposes $R_{\parallel}$ and R are interchangeable.

Given its experimental importance, we would certainly like to find an expression for the end-to-end distance as a function of L, l_p and H for an ideal chain, which seems to be absent in the existing literature. As long as $L \gg \lambda$, the formation of deflection segments in strong confinement decouples the behavior of the chain in the directions parallel and perpendicular to the plane of confinement. Thus, in $\mathbf{e}_{\perp}$ the chain configurations are dominated by stochastic collisions of deflection segments with the top and bottom of the slit, irrespective of the horizontal position of the chain. However, since the parallel axes contain no impediments, the chain is free to swell horizontally and perform some type of two-dimensional random walk.[6,9] As stated in the outset, this assumption is similar to

Daoud and de Gennes' blob theory,[15] and forms the basis of several Flory theories used to explain the behavior of real chains in the Odijk regime.[6,9] However, instead of a two-dimensional walk of blobs, in the strong confinement, we have a two-dimensional walk of deflection segments.

Moving to express these ideas more formally, dimensional analysis reveals that the square end-to-end distance is a function of L/l_p and λ/l_p only

$$\frac{R^2}{{l_p}^2} = f\left(\frac{L}{l_p}, \frac{\lambda}{l_p}\right) \tag{16}$$

In Eq. 16, the dependence of R on slit height is expressed in terms of λ/l_p only, since λ is the only quantity that depends on H. Hypothesizing that the random walk behavior of the chain is decoupled from the slit height leads us to

$$\frac{R^2}{{l_p}^2} = g\left(\frac{L}{l_p}\right) h\left(\frac{\lambda}{l_p}\right) \tag{17}$$

Here g accounts for the walk in the plane of confinement and h accounts for the excursions of the chain in $\mathbf{e}_\perp$.

We hypothesize that since the chain is wormlike in the bulk, $g(L/l_p)$ also describes a wormlike chain, in contrast to a different type walk such as a random flight. If the chain is indeed wormlike, g can be described by the Kratky-Porod model for a two-dimensional wormlike chain[16,17]

$$g\left(\frac{L}{l_p}\right) = \frac{4L}{l_p}\left[1 - \frac{2l_p}{L}\left(1 - e^{-L/(2l_p)}\right)\right] \tag{18}$$

As an additional check, one may also evaluate the bond autocorrelation function

$$C(s) = \langle \mathbf{u}(s) \cdot \mathbf{u}(0) \rangle \tag{19}$$

where $\mathbf{u} = \partial\mathbf{r}/\partial s$ is a tangent vector to the chain contour. $C(s)$ gives the directional correlation between chain segments as a function of the distance along the backbone of the chain, and for an

ideal, 2D wormlike chain is given by [16,17]

$$C(s) = \exp\left(-\frac{s}{2l_p}\right) \tag{20}$$

Notably, the characteristic decay length for a 2D wormlike chain is twice the persistence length l_p of a wormlike chain in bulk solution.

To complete our description of the end-to-end distance, we still need to account for the change in R due to the change in slit height. Because $H \ll l_p$, the dimensionless quantity λ/l_p is small and $h(\lambda/l_p)$ may be expressed as a series expansion

$$h\left(\frac{\lambda}{l_p}\right) = 1 - 2\alpha_R \frac{\lambda}{l_p} + \mathrm{O}\left[\left(\frac{\lambda}{l_p}\right)^2\right] \tag{21}$$

where we define α_R to be a positive constant. We expect this approximation to be very good for large l_p, similar to Eq. 8 for the projected contour length.

Combining Eq. 1, Eq. 18 and Eq. 21 gives

$$R^2 = 4Ll_p\left[1 - \frac{2l_p}{L}\left(1 - e^{-L/(2l_p)}\right)\right]\left[1 - 2\alpha_R\left(\frac{H}{l_p}\right)^{2/3}\right] \tag{22}$$

where we have dropped the second order terms in λ/l_p. In addition to providing a quantitative prediction, Eq. 22 implies that we can distinguish between two subregimes based on the projected contour length of the chain. For $L \ll 2l_p$, we find an "Odijk–rod" regime where the chain behaves like a stiff rod in the plane of confinement. Simplifying Eq. 22 in the rod limit gives

$$R = L\left[1 - \alpha_R\left(\frac{H}{l_p}\right)^{2/3}\right] \tag{23}$$

where the Taylor series expansion $\sqrt{1-\lambda/l_p} \approx 1 - \lambda/2l_p$ has been used to approximate the square root function to first order in λ/l_p. Alternatively, when $L \gg 2l_p$, we encounter an "Odijk–Gaussian" regime where the chain obeys a random walk in the plane of confinement. Here Eq. 22

simplifies to

$$R = 2(Ll_p)^{1/2}\left[1 - \alpha_R\left(\frac{H}{l_p}\right)^{2/3}\right] \tag{24}$$

Note that the "rod" and "Gaussian" terminology employed here reference the rod-like and Gaussian-like regimes of dilute-solution ideal wormlike chains, typically associated with the Kratky-Porod model.[25,27]

2.2 Real Chains

Up to this point, we have limited our discussion to ideal chains. We now abandon this assumption and consider a polymer with a hardcore diameter w confined in a slit of height H. Fortunately, the effects of excluded volume interactions are suppressed for very stiff chains and many of the results of Section 2.1 are directly applicable. Indeed, if we consider a chain shorter than $2l_p$, intra-chain interactions are negligible, and the equations contained in Section 2.1 for the projected contour length, confinement free energy and end-to-end distance remain valid.

For chains longer than $2l_p$, the impact of excluded volume can no longer be neglected. Here, the effects of stiffness on the in-plane walk are diminished, and the conformation becomes much more likely to experience intra-chain interactions. We expect that both the experimentally relevant, end-to-end distance and the confinement free energy of the chain will be sensitive to these interactions. For example, in Section 2.1, we demonstrated that for large values of L, the end-to-end distance of an ideal chain scales like $L^{1/2}$ in a subregime we labelled "Odijk-Gaussian." As indicated in Figure 1, we expect to recover this regime for real chains when $H \gg w$. However, when H approaches w, we expect the polymer size to scale like $L^{3/4}$, the Flory scaling for a self-avoiding walk in two-dimensions.[15,17]

Two Flory theories have appeared in the literature in an attempt to explain the effect of excluded volume on a long chain in strong, slit-like confinement.[6,9] Despite their well-known shortcomings in describing free energies,[28–30] both Flory theories provide insight into the crossover from Gaussian to self-avoiding behavior.

Dai *et al.*[9] have proposed a theory based on the idea of mapping a chain to a two-dimensional projection on the plane of confinement. In their model they define a projected contour length equivalent to Eq. 8 and an empirically–defined, projected persistence length, $l_{p,\|}$, which varies smoothly between l_p and $2l_p$. Two-dimensional excluded volume interactions are then expressed in terms of an excluded area[9]

$$a_{\text{ev}} = l_{p,\|}^2 + 1.3wl_{p,\|} \tag{25}$$

For our purposes, we note that since $w \leq H \ll 2l_p$, the second term in Eq. 25 is at least an order of magnitude smaller than the first. This reduces the excluded area to

$$a_{\text{ev}} = l_{p,\|}^2 \tag{26}$$

which is the same as the excluded area which Hsu *et al.* used for a wormlike chain confined to a flat plane.[17]

Using Eq. 26, one may write a Flory free energy describing a virtual two-dimensional chain[9,17]

$$\frac{F}{k_BT} \sim \frac{R_\|^2}{L_\| l_{p,\|}} + N_{l_{p,\|}}^2 \frac{l_{p,\|}^2}{R_\|^2} \tag{27}$$

where $N_{l_{p,\|}} = L_\|/l_{p,\|}$ is the number of persistence lengths of the virtual chain. By minimizing Eq. 27 with respect to $R_\|$ one finds a polymer size

$$\frac{R_\|}{l_{p,\|}} \sim \left(\frac{L_\|}{l_{p,\|}}\right)^{3/4} \tag{28}$$

which gives the needed $3/4$ scaling for a self-avoiding walk. While the latter Flory theory is appealing, Hsu *et al.* have elegantly shown that the theory embodied in Eq. 27 lacks a crossover to $L_\|^{1/2}$ for any chain length or excluded volume strength.[17] As such, we are unable to recover the ideal chain limit for $H \gg w$ using such a model.

An alternative Flory theory by Odijk postulates an excluded volume based on isotropic inter-

actions between $N_\lambda = L/\lambda$ deflection segments,[6]

$$v_{\text{ev}} = \lambda^2 w \tag{29}$$

As we will see, the three-dimensional nature of the excluded volume expressed in Eq. 29 gives a crossover with an explicit dependence on w/H.

Following Odijk's approach, we write[6]

$$\frac{F}{k_B T} \sim \frac{L}{\lambda} + \frac{R^2}{2Ll_p} + \frac{L^2 w}{R^2 H} \tag{30}$$

where Eq. 30 includes an additional term for the confinement of deflection segments (see Section 2.1). Note that the L/λ term dominates the others, but falls out when differentiating with respect to R.[31] It also is convenient for a future comparison to include a factor of 2 alongside l_p in Eq. 30, since $2l_p$ is the correlation length for a 2D wormlike chain. Differentiating and solving for the in-plane end-to-end distance yields

$$\frac{R}{l_p} \sim \left(\frac{L}{2l_p}\right)^{1/2} \left(\frac{Lw}{2l_p H}\right)^{1/4} \tag{31}$$

This result immediately shows the desired dependence on w/H, and we follow Odijk in defining an excluded volume parameter[6]

$$z \equiv \left(\frac{Lw}{2l_p H}\right)^{1/2} \tag{32}$$

Thus when $z \gg 1$ the polymer size of the scales like $L^{3/4}$ and when $z \ll 1$, the polymer shows ideal scaling

$$\frac{R}{l_p} \sim \left(\frac{L}{2l_p}\right)^{1/2} \tag{33}$$

Comparing the result for ideal chains in Odijk's theory in Eq. 33 with Eq. 24 from Section 2.1 is instructive, since they must agree when $w \ll H$. Here we find that Odijk's theory agrees in part with Eq. 24. Recall that Eq. 24 was a result of a decomposition into two functions $R = g(L/l_p)h(\lambda/l_p)$,

where g accounted for the random walk and h accounted for the fluctuations of the deflection segments in the axis normal to the plane of confinement. Aside from an unimportant difference in prefactor, Eq. 33 agrees with the function $g(L/l_p)$, but neglects the term due to $h(\lambda/l_p)$. In other words, Odijk's Flory theory correctly accounts for the physics of the two-dimensional walk only and neglects the (admittedly small) effect due to the change in deflection length when the slit height changes. We postulate that the same decomposition can be done for chains with excluded volume

$$\frac{R^2}{{l_p}^2} = \tilde{g}\left(\frac{L}{l_p}, \frac{w}{H}\right)\tilde{h}\left(\frac{\lambda}{l_p}\right) \tag{34}$$

Using Eq. 31 to obtain $\tilde{g}$ and our analysis from Section 2.1 to obtain $\tilde{h}$ gives

$$R = c(Ll_p)^{1/2}\left(\frac{Lw}{2l_pH}\right)^{1/4}\left[1 - \alpha_R\left(\frac{H}{l_p}\right)^{2/3}\right] \tag{35}$$

for $z \gg 1$, where c is some O(1) prefactor.

In addition to the effect on R, excluded volume interactions should also impact the free energy of confinement for strongly confined chain. Even with the aforementioned shortcomings in describing free energies,[28–30] Odijk's Flory theory expressed in Eq. 30 provides considerable insight. Substituting Eq. 31 into Eq. 30 gives

$$F \sim \frac{L}{\lambda} + \left(\frac{Lw}{2l_pH}\right)^{1/2} \tag{36}$$

which shows two terms. The first term is due to the confinement of an ideal chain derived in Section 2.1. The second term is due to binary collisions between deflection segments and is equivalent to z. It is the second term that is problematic, due to the neglect of chain connectivity in the mean field approximation inherent in the Flory theory.[28,30] Instead, directly analogous to a self-avoiding walk, this term becomes linear in the contour length with some unknown functional dependence on the excluded volume strength.[28,30] Defining an excess free energy as the free energy difference between the confined chain with excluded volume and the confined ideal chain, one can formally

express this as

$$\Delta F_{\text{ex}} \equiv F - F_{\text{id}} = \frac{L}{l_p}\mu_{\text{ex}}\left(\frac{w}{H}\right) \tag{37}$$

where $\mu_{\text{ex}}(w/H)$ is the excess chemical potential.

In summary, due to the influence of excluded volume interactions, we can now identify a third subregime within the Odijk regime, in addition to the regimes discussed in Section 2.1. We label this regime an "Odijk-Flory" regime, in analogy to the "Odijk-Gaussian" regime for ideal chains. Here, chains longer than Hl_p/w show swollen coil behavior with a size given by Eq. 35 and an excess free energy given by Eq. 37. For the reader's convenience all of the regimes and subregimes discussed in Section 2 are summarized in Table 1.

Table 1: Regimes of strongly confined chains in slits

	bulk	orientation	Odijk		
			Rod	Gaussian	Flory
	$L \ll H$	$H \ll L \ll \lambda$	$\lambda \ll L \ll 2l_p$	$2l_p \ll L \ll l_pH/w$	$l_pH/w \ll L$
$L_\parallel$	$\frac{\pi L}{4}$	Eq. 7		Eq. 8	
R	L	L	Eq. 23	Eq. 24	Eq. 35
$\beta\Delta F_c$	Eq. 9	Eq. 10		$\frac{L}{\lambda}$	$\frac{L}{\lambda}+\frac{L}{l_p}\mu_{\text{ex}}$

3 Simulation Results

3.1 Model and Methods

Having laid out a theory for the Odijk regime in slits, we examine its validity by numerical simulation. To model semiflexible chains, we use a discrete wormlike chain model (DWLC), which is a straightforward discretization of the continuous wormlike chain model used in Section 2.[25,27,32–34] The main advantage of such a fine-grained model is the ability to resolve sub-persistence length features, which are critical to the study of polymers in the Odijk regime, since deflection segments

may be substantially smaller than the persistence length.[20] In our implementation, the polymer is described as a series of beads connected by N bonds of fixed length a giving a contour length $L = aN$. Let the vector $\mathbf{r}_i = (x_i, y_i, z_i)$, $i \in [1, N+1]$ describe the positions of the beads along the contour and let $\mathbf{u}_i = (\mathbf{r}_{i+1} - \mathbf{r}_i)/a$ be the unit vector of the i^{th} bond. In the DWLC model a bending potential is enforced between consecutive bonds

$$U_{\text{bend}} = k_B T \kappa \sum_{i=1}^{N-1} (1 - \mathbf{u}_{i+1} \cdot \mathbf{u}_i) \tag{38}$$

with a bending elasticity κ. The persistence length may be expressed in terms of κ by considering the equilibrium probability density function for the bond angle of an ideal wormlike chain[27]

$$\frac{l_p}{a} = \frac{1}{2} \frac{\kappa - 1 + \kappa \coth \kappa}{\kappa + 1 - \kappa \coth \kappa} \tag{39}$$

Note that we take the relation between the bending constant and the persistence length embodied in Eq. 39 as the definition of the persistence length, rather than the characteristic length scale of decay of the correlation between successive bonds. As has been discussed by Hsu *et al.*,[35] these definitions are only equivalent when the chain has no excluded volume, and we find that Eq. 39 conveniently separates the effects of stiffness due to bending elasticity and stiffness due to proximal intra-chain interactions.

We consider both ideal and real chains, where real chains are endowed with excluded volume interactions between chain segments. This is accomplished by considering spherical beads located at bond joints with hard core repulsion potential described by

$$U_{\text{ev}}(\mathbf{r}_{ij}) = \sum_{i=1}^{N} \sum_{j=1}^{i-1} \begin{cases} \infty, & |\mathbf{r}_{ij}| \leq w \\ 0, & |\mathbf{r}_{ij}| > w \end{cases} \tag{40}$$

where w is the bead radius and $|\mathbf{r}_{ij}|$ is the distance between the centers of beads i and j. While it appears from Eq. 40 that w is a freely varying parameter, unphysical chain-crossing occurs when w

is less than the bond length a. Accordingly, we choose to set $w = a$, resulting in a chain composed of osculating hard spheres. Notably, the choice of a hard core potential also increases the speed of the algorithm.

Both ideal and real chains must also interact with the slit walls. Similar to the excluded volume interaction, chains interact with confinement via a hard potential

$$U_{\text{wall}}(\mathbf{r}) = \sum_{i=1}^{N} \begin{cases} \infty, & |\mathbf{r}_i \cdot \mathbf{e}_\perp| \geq H/2 \\ 0, & \text{otherwise} \end{cases} \tag{41}$$

where $\mathbf{r}_i$ is the vector from the origin to the center of bead i, and H is the slit height. Note that Eq. 41 confines the centerline of the chain, and that this potential corresponds to a physically larger channel for a polymer with excluded volume interactions. For our hard-bead model, this means that the "true" slit height is $H + w$, if we assume that the bead–wall interaction is the same as the bead–bead interaction.[11–13,34] A hard potential is of course an approximation, and in a real experimental system both the interaction potential and the notion of an effective slit height become more complicated. We expect this approximation to break down as the length scales w and H converge, and therefore recommend caution in interpreting our results when $w \approx H$. Notice further that the notation for the slit height used here is different than in our previous work where the true slit height was denoted by H and centerline confinement was given as an effective slit height, H_{eff}.[24,25,34,36]

We calculate equilibrium properties of the DWLC model using an off-lattice implementation of the pruned-enriched Rosenbluth method (PERM).[18,25,27] PERM is a chain growth Monte Carlo algorithm with many advantages over conventional Markov-chain algorithms for very long chains in confinement, since the relaxation time of chains in the latter class of algorithms scale as $\mathrm{O}(N^2)$.[25] Additionally, PERM natively obtains properties as a function of chain length, which is especially useful for the problem at hand.

In the present manuscript, self-avoiding chains are grown up to $5 \times 10^4 + 1$ beads on a DELL

Linux cluster using a master/slave parallel algorithm as in our previous work.[25,27] Static properties were calculated using $\approx 10^5$ tours, which is sufficient to ensure that the standard error of most properties are smaller than the plotted symbol size, unless otherwise noted. In order to streamline future discussion, Table 2 outlines the specific data sets referenced in Sections 3.2 and 3.3.

Table 2: PERM data sets

		Confined Ideal Chains		
	L/a	l_p/a	H/a	# Tours $\times 10^5$
set 1	[1, 50001] [a]	5000	(5, 500) [b]	10.5
set 2	[1, 50001]	(50, 5000)	5	25.5
set 3 [c]	[1, 50001]	$(10^{1.5}, 10^{3.5})$	(1, 100)	5.5
set 4 [d]	[1, 50001]	{5, 50, 500, 5000}	(50, 500)	0.5
		Confined EV Chains		
	L/w	l_p/w	H/w	# Tours $\times 10^5$
set 5	[1, 50001]	(50, 5000)	5	5.5
set 6 [c]	[1, 50001]	$(10^{1.5}, 10^{3.5})$	(1, 100)	11
		Unconfined EV Chains		
	L/w	l_p/w		# Tours $\times 10^5$
set 7	[1, 50001]	$(10^{1.5}, 10^{3.5})$		5.5

[a] Linearly spaced ranges are denoted with square braces; [b] Logarithmically spaced ranges are denoted with round braces; [c] Data vary such that H/l_p is a constant value at $10^{-1.5}$; [d] Runs were performed for the given range of H/l_p at each of these values of l_p/a.

We are specifically interested in calculating polymer properties relevant for the theory of strongly confined chains presented in Section 2. Most of the properties of interest are calculated in a straightforward manner by discretizing their previously given definitions. However, there is some art to efficiently calculating static properties in PERM and further details can be found in our previous work.[25,27]

For clarity's sake, a brief discussion of the free energy calculations in PERM is also warranted.

In PERM, the free energy

$$\Delta F(n) = k_B T \ln \frac{\langle W(n) \rangle}{\langle W_0(n) \rangle} \tag{42}$$

is obtained from a ratio of the Rosenbluth weight of the n^{th} bead of the chain $W(n)$ and the Rosenbluth weight of an ideal, wormlike chain in the bulk $W_0(n)$.[18,24,25,27] In other words, the reference state for the free energy is an ideal, wormlike chain. To obtain the confinement free energy of an ideal chain, this reference state is sufficient, and ΔF_c can be obtained from Eq. 42 in a single simulation.

The introduction of excluded volume interactions complicates the picture however, since the confinement free energy for a real chain has a real chain reference state. In this case, the free energy of confinement requires a simulation of a chain with excluded volume in the bulk in addition to the confined chain calculation. Therefore, we first perform a simulation of a confined chain with excluded volume and use Eq. 42 to obtain $\Delta\tilde{F}$. Then, we evaluate Eq. 42 in a simulation of a real chain in the bulk to obtain $\Delta\tilde{F}_0$. The confinement free energy of a chain with excluded volume is then obtained as a difference between these free energies

$$\Delta\tilde{F}_c = \Delta\tilde{F} - \Delta\tilde{F}_0 \tag{43}$$

To obtain the excess free energy of a confined chain a similar subtraction procedure is performed to change the reference state to a confined, ideal chain. Here, the excess free energy is the difference between the result of a simulation of a confined chain with excluded volume and a confined, ideal chain

$$\Delta F_{\text{ex}} = \Delta\tilde{F} - \Delta F_c \tag{44}$$

3.2 Ideal Chains

We are now prepared to compare results from PERM simulations to the predictions contained in Section 2 for the Odijk regime in slits. As was the case in Section 2.1, in this section we neglect any effects due to excluded volume and examine ideal chains.

We begin by attempting to verify the existence of the weak confinement and orientation regimes for $L \ll H$ and $H \ll L \ll \lambda$ respectively. To this end, Figure 2(a) shows the projected contour length for various values of H/l_p as a function of chain length. The agreement with both the functional form and prefactors of the theory in Section 2.1 is excellent. As expected the projected contour length follows Eq. 5 for $L \ll H$, transitions near $L \approx H$ and then follows Eq. 7 for $L \gg H$. The data fall off of Eq. 7 at even larger values of L, presumably as the chain enters the Odijk regime. This presumption is supported by the fact that chains with smaller H/l_p values follow Eq. 7 for longer chain lengths, suggesting that the width of the orientation regime is governed by the deflection segment length.

Figure 2(b) shows a similar story for the confinement free energy versus contour length. For chains much smaller than H the data show excellent agreement with Eq. 9, again without any fitting parameters. The data transition at $L \approx H$ and follow Eq. 10 for chains much greater than H. As is the case for the projected contour length, the width of the orientation regime depends on the ratio of H/l_p. This observation again supports the fact that the upper bound is determined by the deflection segment length, as discussed in Section 2.1.

To examine the transition to the Odijk regime more closely, we focus on Figure 3(a), which rescales the data shown in Figure 2(a) for the projected contour length as a function of chain length. The data in the figure are again consistent with the ideal chain theory presented in Section 2.1. Just as in Figure 2(a), the portion of the curve for $L \ll \lambda$ agrees quantitatively with the theory for the orientation regime in Eq. 7. Around $L \approx \lambda$ the data transition towards Odijk scaling, and for $L \gtrsim 10\lambda$ it appears to have reached the "long-chain limit." In this limit, when $L \gg \lambda$, the data converge to a value of $\alpha_L = 0.09137$, consistent with prior calculations by Burkhardt *et al.*[11–13]

In addition to the data as a function of chain length, Figure 3(b) extracts the longest chain lengths in panel (a) and replots them as a function of H/l_p. The agreement between these data and Eq. 8 explains why the data in Figure 3(a) collapse for different channel sizes. Furthermore, it appears that Eq. 8 is a good description of the data even for the largest channel sizes in the data set ($H/l_p \approx 0.1$). Therefore, at least for the projected contour length, we can consider the chain to be

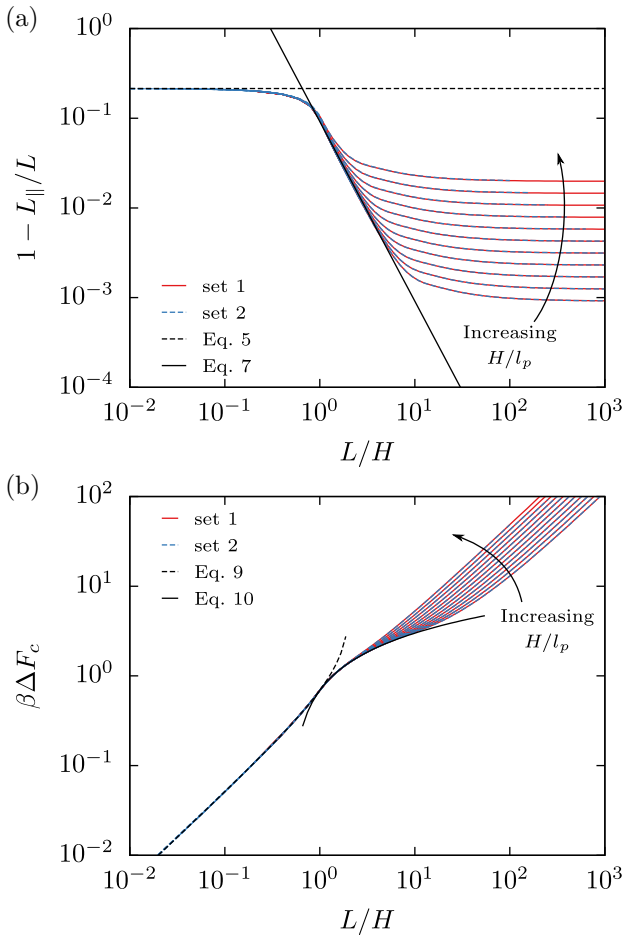

Figure 2: PERM data for (a) the projected contour length of slit-confined, ideal chains and (b) the confinement free energy of slit-confined, ideal chains as a function of chain length. In both panels, simulations are run with either a fixed slit height (solid lines) or a fixed persistence length (dashed lines) which corresponds to set 1 and set 2 in Table 2.

in the Odijk regime even for a rather aggressive value of $H \approx 0.1 l_p$.

As is the case with the projected contour length in Figure 3, Figure 4(a) shows data for the confinement free energy as a function of contour length. The results for the free energy are congruent with both the results for the projected contour length and the theory in Section 2.1. Unlike Figure 2(b), the data for the free energy of confinement in Figure 4(a) are normalized by the number of deflection segments. This causes a peak in the data at $L \approx H$, where the entropic penalty of adding an additional monomer is greatest due to a loss of rotational degrees of freedom. While the peak in Figure 4(a) is at $L \approx H$, it appears to move as H/l_p changes; this effect is caused by scaling the x-axis with respect to λ. As expected, the free energy becomes extensive and proportional to $k_B T$

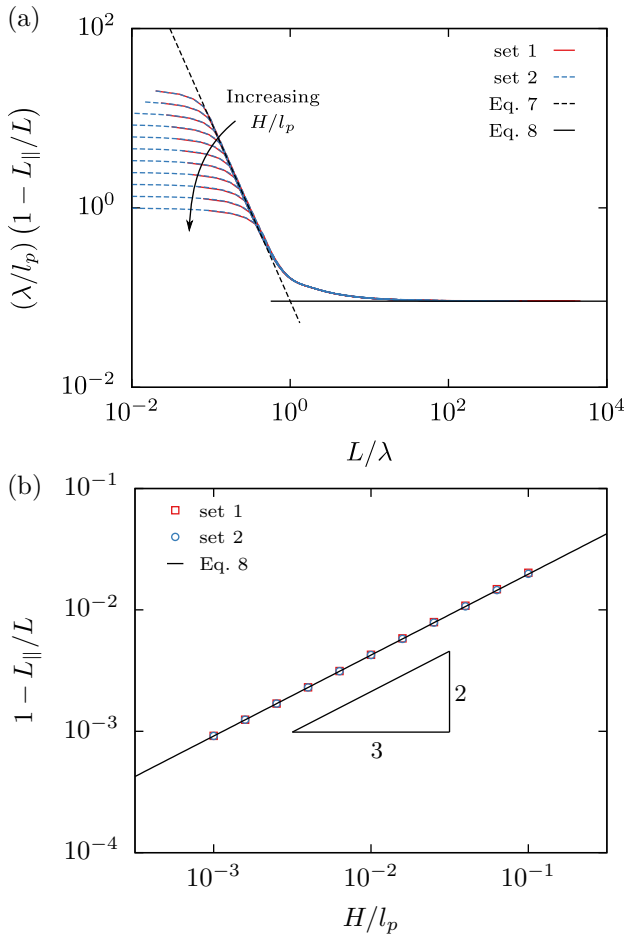

Figure 3: PERM data for the projected contour length of a slit-confined chain versus (a) chain length and (b) normalized slit height (for the largest L only). Simulation data sets include data at a constant slit height (squares and solid lines) and a constant chain persistence length (circles and dashed lines). These data correspond to sets 1 and 2 in Table 2 respectively. The dashed line in the main portion of panel (a) is given by Eq. 7 and the solid curve in (a) and (b) is given by Eq. 8. Because of the rescaled y-axis in panel (a), Eq. 8 reduces to a constant value of 0.09137.

in the long chain limit. It is a satisfying check of our intuition that the free energy is almost exactly k_BT per deflection segment in this limit. As one might also suspect, the free energy approaches the long chain limit asymptotically, and for most practical purposes, the deviation from the asymptote becomes small when $L \gtrsim 10\lambda$.

For very long chains in Figure 4(a), there is some observable spread in the data that appears to disagree with the prefactor of 1.1036 obtained from Burkhardt *et al.*[11–13] This apparent disagreement is due to the finite values of H/l_p used in the PERM simulations. The inset to Figure 4(a) shows the largest chain lengths in the main panel, replotted versus H/l_p and compared to the pref-

actor from Burkhardt *et al.*. The inset shows that for values of $H/l_p \lesssim 10^{-2}$, the PERM data agree very well with a value of 1.1036, but slit heights larger than this deviate below the curve. Thus in contrast to the projected contour length, the free energy is more sensitive to the slit height and one may need to consider smaller ratios of H/l_p to observe Odijk scaling behavior. This can be understood by recognizing that the prefactor for the free energy is an order of magnitude larger than the corresponding prefactor for the projected contour length. Thus terms of order $(\lambda/l_p)^2$ may also make a substantial contribution to the free energy at the values of H/l_p in the simulation data set.

Figure 4(b) examines the dependence of the free energy on H/l_p even further. Here, simulation data for the confinement free energy per persistence length for chains of length $L/a = 50001$ are shown versus a much larger range of H/l_p than in panel (a). When the data is plotted this way, one can compare to the interpolation formula of Chen and Sullivan[14] (Eq. 13) in addition to Eq. 12. For larger slit heights, the PERM data show a smooth transition from Odijk scaling when $H \ll l_p$ to ideal scaling when $H \gg l_p$, similar to the results of Chen and Sullivan using polymer field theory.[14] Across the entire range of confinement strengths the PERM data agree very well with Eq. 13. When the free energy is normalized with the persistence length, $H/l_p \approx 0.1$ appears to denote the onset of Odijk scaling, in contrast to the results in the inset of panel (a). This discrepancy is due to the difference in scaling of the y-axis, which in panel (a) divides by the small term λ/l_p.

We now turn our attention to the theory in Section 2.1 for the projected size of the confined chain. Recall that in Eq. 15, we used a simple trigonometric argument to claim that the projected size, $R_{\|}$, was equivalent to the conventional end-to-end distance for large R. Figure 5 shows PERM data for the relative error in this approximation versus R/H. For small values of R/H the relative error remains O(10^{-1}) but falls precipitously for $R \gg H$. The slope of -2 evident on the right hand side of the figure is consistent with the prediction from Eq. 15. From the figure, it is clear that $R \approx R_{\|}$ is excellent for values of $R \gtrsim 10H$.

Having established that R is a reasonable metric, we would like to validate the key assumptions of our theory. Recall that in Section 2.1 we postulated that the function describing R could be

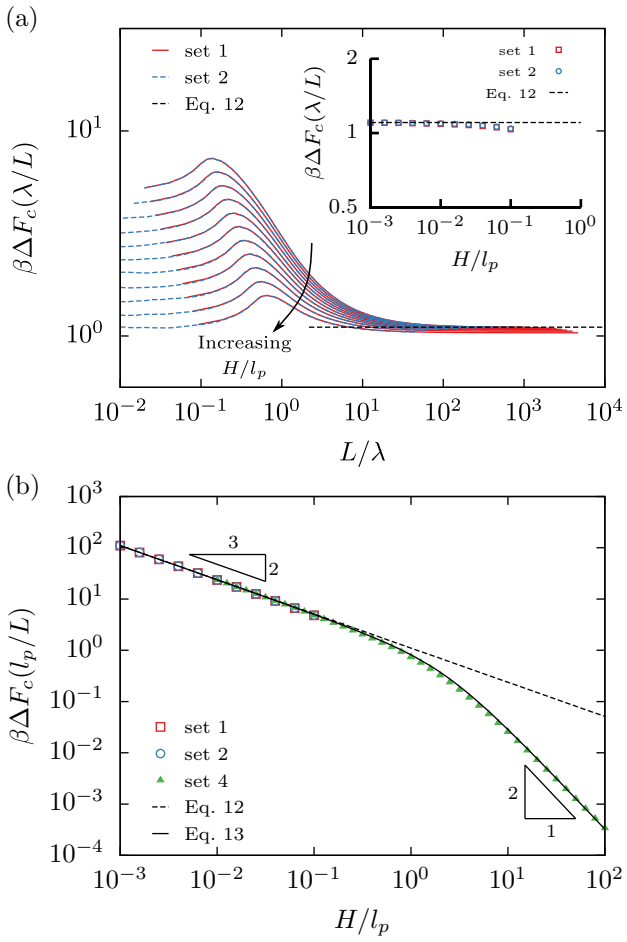

Figure 4: PERM data for confinement free energy of a slit-confined chain (a) normalized by the number of deflection segments and (b) normalized by the number of persistence lengths. The data in the main panel (a) are shown versus the number of deflection lengths and versus H/l_p in the inset. The data in panel (b) are shown versus H/l_p. Simulation data sets include data at a constant slit height (squares and solid lines), constant chain persistence length (circles and dashed lines), and variable slit height and persistence length (filled triangles). These data correspond to sets 1, 2 and 4 in Table 2 respectively. Note that the dashed line in panel (a) corresponds to Eq. 12, which reduces to a constant value of 1.1036.[11–13]

decomposed into some function $g(L/l_p)$ describing a random walk and another function $h(\lambda/l_p)$ to account for the deflection segments. Focusing on $g(L/l_p)$ for the moment, we postulated that the confined chain could be approximated as a two-dimensional walk of persistent segments, *i.e.* a 2D wormlike chain.

To test this hypothesis, Figure 6 shows simulation results for the bond autocorrelation function $C(s)$ for simulations at various values of H/l_p. In order to collapse the data to a single curve, the

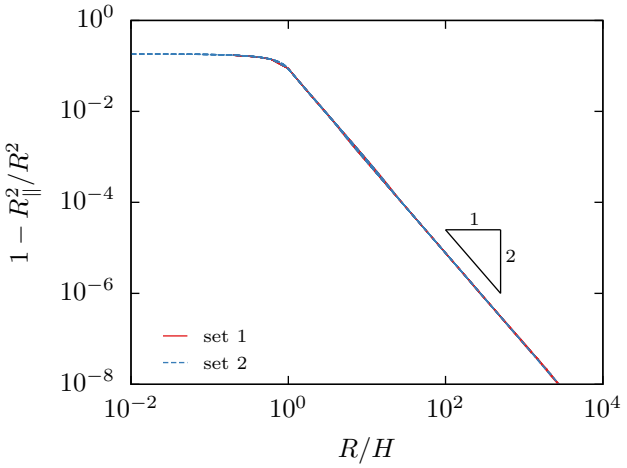

Figure 5: Simulation data for the relative error between $R_\parallel$ and R as a function of the rms end-to-end distance of the chain.

autocorrelation function in Figure 6 has been rescaled by the power l_p/λ. The collapse is very good, and as expected from Eq. 20, the bond correlations for $s \gg \lambda$ decay exponentially with a characteristic length of $2l_p$. This is indicative of a two-dimensional wormlike chain and provides confirmation of our hypothesis.

However, as was the case with the confinement free energy and the projected contour length, there is also some nuance to the behavior of $C(s)$ as a function of the distance along the contour. In Figure 6, we observe that for $s \ll \lambda$ the correlations decay with a characteristic length of l_p, exactly half of the value observed for large s. Of course, the relationship $C(s) = \exp(-s/l_p)$ shown by the dashed line in the figure is exactly what one would expect for an unconfined, three-dimensional wormlike chain. Thus, the chain is experiencing correlations indicative of bulk, 3D behavior on length scales much less than λ and confined, 2D behavior on length scales much greater than λ. In addition to the interest to the problem at hand, this result provides a satisfying example of an oft-made assumption that properties below the scale of confinement can be treated as effectively bulk-like.

Additionally, the results encapsulated in Figure 6 are somewhat at odds with previous work, which discuss bond correlations in terms of a projected persistence length, $l_{p,\parallel}$, that depends on H/l_p.[9] However, there are at least two good explanations as to why our data disagree. First, up to

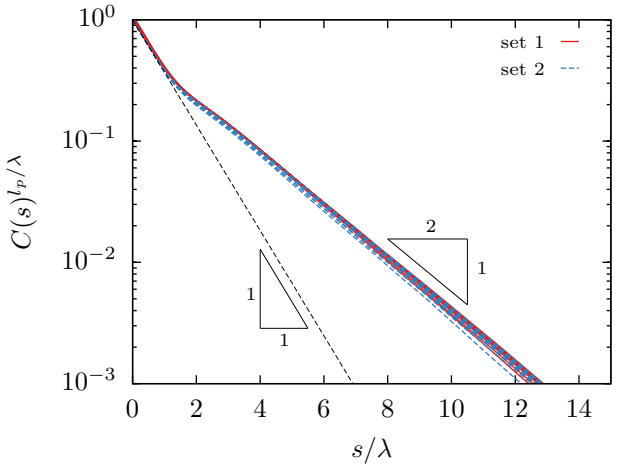

Figure 6: Simulation data for the bond autocorrelation function $C(s)$ versus contour distance s for various values of H/l_p. The data presented in this figure correspond to sets 1 and 2 in Table 2. The autocorrelation function has been rescaled by a power of l_p/λ in order to collapse all of the data to a single curve. The dashed line depicts the curve $C(s) = \exp(-s/l_p)$.

this point, we have not considered the effect of excluded volume as was done in prior work. Indeed, Hsu *et al.* have shown that simple relationships between various definitions of the persistence length break down upon inclusion of excluded volume.[35] Secondly, and more importantly, the authors of the previous study consider a much wider range of values of H/l_p, whereas we limit ourselves to the Odijk regime, where $H \ll l_p$. If we also restrict the equations provided in Ref. 9 to the Odijk regime, we find that Eq. 20 and the results in Figure 6 are both in good agreement.[9]

Having confirmed that the random walk is indeed wormlike, we proceed to test the predictions of Eq. 18 for $g(L/l_p)$ versus the values of R obtained form our PERM simulations. Accordingly, Figure 7(a) shows PERM simulation data compared to Eq. 18 for a range of values of H/l_p. Note that Eq. 18 is simply the result for the end-to-end distance of a 2D wormlike chain[16,17] and does not include any dependence on the slit height. The data agree very well with Eq. 18, and the curves are practically indistinguishable except for some notable sampling error that accompanies simulations of extremely large chains in PERM. In fact, at first glance it appears that the simulation data are in quantitative agreement with the prediction even without accounting for the dependence on H/l_p.

To investigate this further, the inset in Figure 7(a) shows the relative error between R^2 and g by

plotting

$$1 - \frac{R^2}{l_p^2}\frac{1}{g} = 1 - h\left(\frac{\lambda}{l_p}\right) \tag{45}$$

as a function of the number of deflection segments for different values of H/l_p, where we have used Eq. 17 as our definition for h. As anticipated, there is a small, but systematic deviation in the data as a function of H/l_p. To explain this deviation, we anticipated in Section 2.1 that h could be expressed as the series expansion given by Eq. 21. Using Eq. 21 as a guide, we rescale the relative error by by λ/l_p and obtain Figure 7(b). The collapse of the data is excellent (again with some notable sampling error for long chains), showing that the first-order terms are sufficient to capture the dependence of R^2 on H/l_p. Additionally, a fit to the data in the range $L/\lambda \in [1,10]$ yields a value of $\alpha_R = 0.1039(5)$, which completes the expression for the square end-to-end distance in Eq. 22.

Since Eq. 22 appears to quantitatively describe the end-to-end distance, it should estimate the in-plane size from a polymer's free solution molecular weight, persistence length and the slit height. This should be an excellent approximation for long chains, since we believe the difference to be minimal between $R_\parallel$ and R when $R \gg H$. In addition, since the value of α_R is O(10^{-1}) and $\lambda/l_p \ll 1$, Eq. 18 should also be an excellent approximation for $R_\parallel$, as is evident in Figure 7(a). Other useful approximations are contained in Equations 23 and 24 which contain assumptions about the contour length as described in Section 2.1. These equations are also displayed in Figure 7(a).

Finally, we close this section with a comment about an alternative theory, which we label the "projected 2D chain theory".[9] In this theory, the statistics of the three-dimensional chain are interpreted in terms of a mapping to a two-dimensional chain. The parameters of the mapping are $L_\parallel$ and $l_{p,\parallel}$, the contour length and persistence length of a chain projected onto the surface of confinement. Similar to Section 2.1, the projected 2D chain theory describes the chain as a two-dimensional walk, making the difference between the two theories subtle to distinguish. The key difference lies in the dependence of the chain statistics on H/l_p, which is embedded in the parameter $L_\parallel$ (as seen in Figure 3) for the projected 2D chain theory and is independent of L for

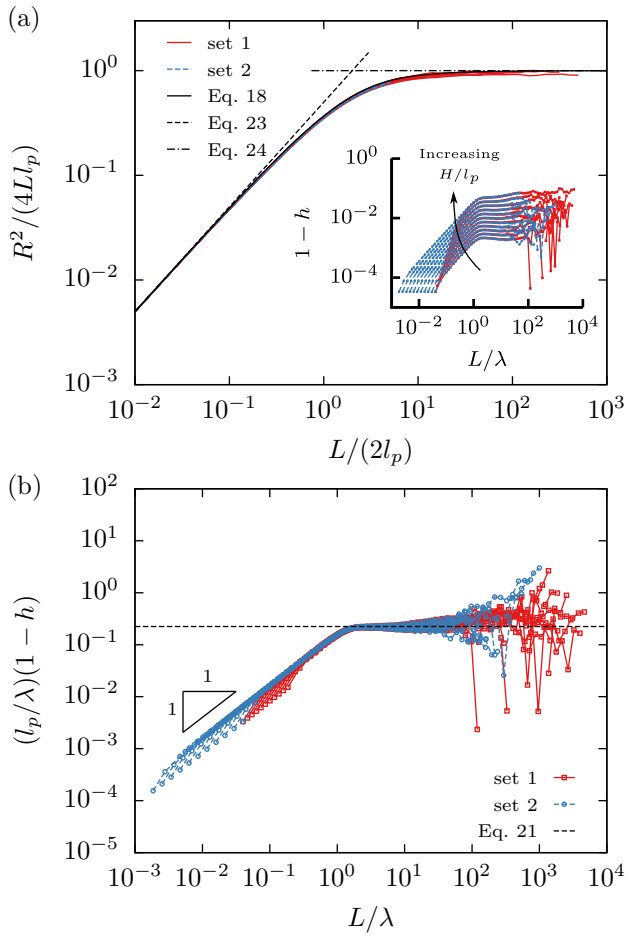

Figure 7: Simulation data for the end-to-end distance of ideal chains as a function of contour length. The data in the figure correspond to sets 1 and 2 in Table 2. The data in panel (a) is scaled by the size of an ideal, 2D chain. The solid curve in panel (a) corresponds to $g(L/l_p)$ given by Eq. 18, the dashed curve gives Eq. 23 and the dot-dashed curve gives Eq. 24. The inset to panel (a) shows the relative error by approximating $R \approx g$ without including a dependence on the slit height. Panel (b) shows a rescaled value of the relative error which accounts for the first term in the series expansion of $h(\lambda/l_p)$ in Eq. 21. The dashed line shows the prediction of Eq. 24 with a value of $\alpha_R = 0.1039(5)$.

our treatment in Section 2.1.

Since we have calculated R^2, $L_\parallel$ and $l_{p,\parallel}$, we are in a position to evaluate the claims of the projected 2D chain theory respecting the dependence of R^2 on H/l_p. According to the theory, the crossovers between subregimes depends on the value of $L_\parallel/l_{p,\parallel}$ rather than L/l_p. Therefore, since $L_\parallel$ depends on H/l_p, one would expect a weak slit height dependence on the crossover between subregimes. However, the data collapse in Figure 7(b) does not support this interpretation, since we

have assumed that h is independent of L/l_p. Additionally, the projected 2D chain theory predicts that the dependence of R on H/l_p changes between subregimes, because $R \sim L$ for the Odijk-rod subregime and $R \sim L^{1/2}$ for the Odijk-Gaussian subregime. By contrast, the collapse in Figure 7(b) shows that the dependence of R on slit height is independent of the change in subregime. Finally, there is a statistically significant (albeit small) difference between the values of the constants α_R and α_L. This difference provides further evidence that the slit height dependence of $L_\parallel$ cannot completely account for the slit height dependence of R.

3.3 Real Chains

Building on our discussion of ideal chains, we now turn our attention to the results of PERM simulations which incorporate excluded volume effects. As Section 2.2 indicates, one expects the impact of excluded volume to be minimal on the behavior of short chains and on metrics which depend solely on proximal chain-chain interactions. In agreement with this hypothesis, we do not observe changes to $L_\parallel$ following the inclusion of excluded volume interactions, and we therefore omit it from further discussion. However, we do expect a change in behavior for metrics such as the end-to-end distance and confinement free energy, which depend on interactions between distal polymer segments. Such expectations were outlined in Section 2.2, where we harmonized a Flory theory by Odijk[6] and the theory for ideal chains in Section 2.1.

One of the most apparent predictions of the Flory theory in Section 2.1 is a change in the scaling of the end-to-end distance from $R \sim L^{1/2}$ to $R \sim L^{3/4}$ for self-avoiding chains in the long-chain limit. To test this prediction, Figure 8(a) shows the computed mean square end-to-end distance (normalized by the size of an ideal chain) as a function of the contour length (normalized by $2l_p$). Note that this normalization changes the slope to $R^2/L \sim L^0$ for ideal chains and to $R^2/L \sim L^{1/2}$ for swollen chains. In the figure, the end-to-end distance is calculated at a fixed value of H/l_p, while w/H is free to vary. As such, the change in scaling of the polymer size as the excluded volume strength varies is unambiguous, since the degree of freedom due to w/H is absent for ideal chains.

The results shown in Figure 8(a) agree with Odijk's Flory theory and do indeed give a slope

of $1/2$ in the long chain limit. This is most readily apparent for chains where $w \to H$, which show a very short crossover to the self-avoiding behavior. We further anticipate that chains with $w \ll H$ also show a slope of $1/2$ in the long chain limit, but finite computational resources limit our ability to check this hypothesis. In addition to agreement with the slope predicted by scaling theory, the results agree with Eq. 35, describing the end-to-end distance in the so-called Odijk-Flory subregime. Using a least-squares fit to the data in the figure, we obtain the prefactor $c = 0.593(3)$ for Eq. 35, which agrees with our expectation that c should be O(1).

Beyond describing the long-chain limit, Odijk's theory also predicts the crossover behavior according to our original conceptualization of the problem embodied in the schematic in Figure 1(b). The results in Figure 8(a) are in good agreement with this prediction. For chains with $w \ll H$, the behavior very closely resembles the ideal chain case from Figure 7(a) and follows the curve describing the end-to-end distance of an ideal, two-dimensional wormlike chain given by Eq. 18. As w/H increases, the excluded volume strength increases and the curve shows a slope of $1/2$, indicating a two-dimensional self-avoiding walk. Figure 8(b) further examines the crossover in terms of the excluded volume parameter z given in Eq. 32. The data collapse nicely to a single curve in the large z limit, which confirms that Eq. 32 does indeed describe the crossover to self-avoiding chains in the Odijk regime.

In Figure 1 we also proposed that a strongly confined polymer should behave like a two-dimensional, self-avoiding wormlike chain in the limit that $w \to H$. To evaluate this claim, Figure 8(a) and Figure 8(b) also show data from lattice simulations of 2D, self-avoiding wormlike chain from Hsu *et al.*[17] To compare both data sets, it was necessary to compute the persistence length of the lattice chains simulated by Hsu *et al.* in a manner consistent with our approach from Section 3.1. Therefore, instead of using the empirically determined values given in Ref. 17, we used the relation

$$l_p = l_b \left[2 \exp\left(-\frac{\varepsilon_b}{k_B T} \right) \right]^{-1} \tag{46}$$

where l_b is the bond length of the lattice chain and ε_b is the energy penalty for bending. Using this definition of the persistence length and the data for the R^2 versus L in Ref. 17, we find ex-

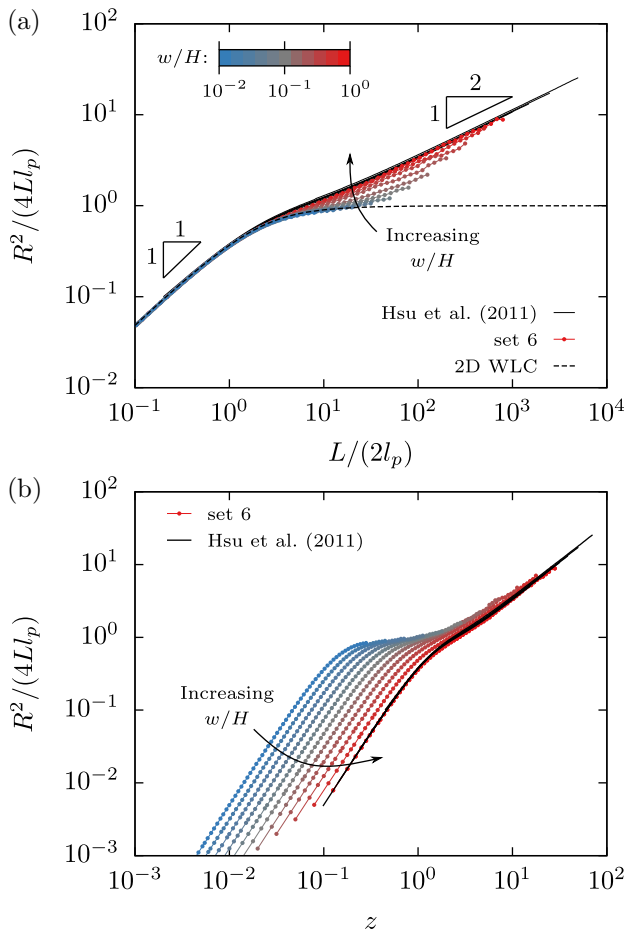

Figure 8: PERM data for the normalized end-to-end distance of real chains as a function of (a) normalized projected contour length and (b) excluded volume parameter. In both panels, simulations are run at a fixed value of $H/l_p = 10^{1.5}$, and the different colored symbols correspond to varying values of w/l_p as indicated by the colorbar. PERM data correspond to set 6 in Table 2. The solid lines in both panels (a) and (b) correspond to data found in Hsu *et al.*[17] for 2D wormlike chains on a lattice.

cellent agreement with the slit data in the limit that $w \to H$. In fact, with no fitting parameters, both the scaling crossover and prefactors agree, providing strong evidence that as the chain width approaches H, the slit-confined chain becomes two-dimensional.

As was the case with ideal chains, we expect that the polymer size will have a weak dependence on the change in deflection segment length as the slit height changes in the form of some function $\tilde{h}(\lambda/l_p)$. In the ideal chain case, we had a closed form expression for $g(L/l_p)$, so we could examine

h by the decomposition

$$h = \frac{R^2}{l_p^2}\frac{1}{g} \tag{47}$$

which is equivalent to its definition in Eq. 17. However, while $g(L/l_p)$ is known for ideal chains, no closed form expression is available for $\tilde{g}(L/l_p, w/H)$ when excluded volume is introduced. We circumvent this problem by performing multiple simulations at constant L/l_p and w/H and look for the relative change in R^2 when the value of λ/l_p is varied.

Defining the relative change in the square end-to-end distance as the difference between R^2 at one value of λ/l_p, and R_0^2 at another, much smaller value of $\lambda_0/l_{p,0}$, we obtain

$$\frac{R_0^2 - R^2}{R_0^2} = \frac{\tilde{g}_0\tilde{h}_0 - \tilde{g}\tilde{h}}{\tilde{g}_0\tilde{h}_0} \tag{48}$$

In Eq. 48, $\tilde{g}$ and $\tilde{g}_0$ cancel as long as we hold L/l_p and w/H constant, which is easily done in PERM. Assuming that $\tilde{h}$ can be expanded like Eq. 21, and dropping terms of order $(\lambda/l_p)^2$ gives

$$1 - \frac{R^2}{R_0^2} = 2\alpha_R\left(\frac{\lambda}{l_p} - \frac{\lambda_0}{l_{p,0}}\right) \tag{49}$$

Note that when $\lambda_0/l_{p,0} \to 0$, $R_0 \to l_p^2\tilde{g}$ and we recover the relative error expression used in Section 3.2.

We proceed to examine $\tilde{h}$ in Figure 9 in a manner similar to our analysis of the ideal function h in Figure 7. Accordingly, the inset shows the relative change in the end-to-end distance, $1 - R^2/R_0^2$, as a function of the number of deflection segments, which does indeed change as we vary H/l_p. Similar to the inset in Figure 7(a), the change is small but systematic. To collapse the data, Eq. 49 is rearranged to rescale the y-axis by dividing by the difference in λ/l_p and the result is shown in the main panel in Figure 9. The data collapse very cleanly for small values of L/λ, but show significant sampling error for larger contour lengths, similar to Figure 7(b). The axis choice in Fig. 9 exaggerates the sampling error, since the relative error between the two measures of R^2 is divided by the difference between two small numbers: λ/l_p and $\lambda_0/l_{p,0}$. A fit to the data in

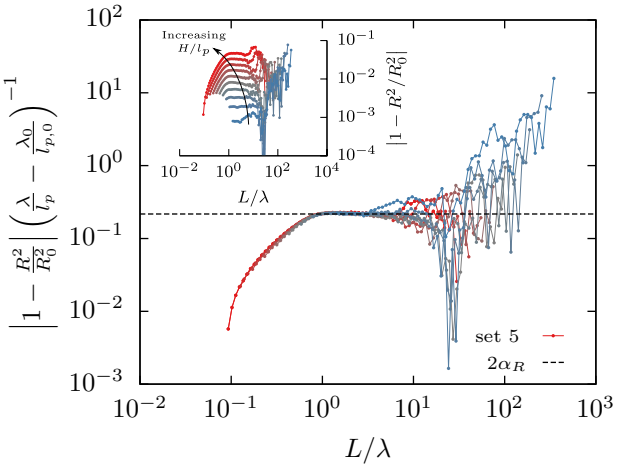

Figure 9: The relative change in square end-to-end distance between simulations with different values of H/l_p as a function of the number of deflection segments. The inset shows the absolute value of the relative change and the main panel shows the absolute value of the relative change scaled by the difference in λ/l_p between the simulations. The absolute value is used since the data are presented on a log scale and sampling error leads to a fluctuation in the sign of the error for large L. The data in the figure were obtained at a constant value of $H/w = 5$ and correspond to set 5 in Table 2. The dashed line in the figure corresponds to a value of 2α. The value of H/l_p varies from 10^{-3} to 10^{-1}.

the range $L \in [1,10]$ gives a value of the constant $\alpha_R = 0.108(1)$, which is close to the value of $0.1039(5)$ for ideal chains obtained in Section 3.2. Indeed the agreement is good, considering that the error estimates given are from fits over limited ranges due to the sampling error for large L. The fact that α_R is similar between real chains and ideal chains parallels the consistency of $L_\parallel$, and provides evidence that the formation of deflection segments is unaffected by the inclusion of excluded volume interactions.

Finally we close this section with a discussion of the free energy of the confined chain. Odijk's theory in Section 2.2 presents two components that contribute to the total free energy of a confined chain with excluded volume relative to an ideal, unconfined reference state

$$\Delta F_{\text{conf,ev}} = \Delta F_c + \Delta F_{\text{ex}} \tag{50}$$

The first is the free energy required to confine an ideal chain, ΔF_c, and the second is the free energy due to excluded volume interactions of the confined chain, ΔF_{ex}. As it often appears in the

literature, it is also convenient to define a free energy of confinement $\Delta\tilde{F}_c$ as the free energy required to confine a chain with excluded volume interactions relative to an excluded volume reference state.

The main panel in Figure 10 shows an example of all three of these free energies (normalized by k_BT) as a function of the number of persistence lengths. Two obvious conclusions jump out from the data. First, we observe that $\Delta F_c \gg \Delta F_{\text{ex}}$, and therefore the free energy required to confine a chain dominates the total free energy. This finding matches our intuition developed from Odijk's Flory theory in Section 2.2. Second, we see that $\Delta F_c \approx \Delta\tilde{F}_c$. This observation is related to the fact that the excess free energy is much smaller than the confinement free energy, but we stress that the statements are not equivalent since $\Delta\tilde{F}_c$ has a different reference state. Nevertheless, since the two confinement free energies are so similar, for most practical purposes the confinement free energy of a chain with excluded volume can be described by Eq. 12, which was originally discussed in terms of the ideal chain only.

While not dominant in terms of magnitude, the excess free energy is still important, since it determines the crossover from Odijk-Gaussian to Odijk-Flory behavior. Thus for small values of L/l_p the excess free energy is practically zero as indicated by the noisy fluctuations about the value of 10^{-4} for $\beta\Delta F_{\text{ex}}$ in Figure 10. However as L/l_p increases, the number of possible intrachain interactions follows suit, and the excess free energy eventually scales linearly in L/l_p, parallel to ΔF_c in the long chain limit. The linear scaling in L/l_p contradicts the Flory theory in Section 2.2, but coincides with the predictions of modern renormalization group theory.[30]

The excess free energy also changes with excluded volume strength, but since Flory theory fails to describe this effect, we are not aware of any theory that makes a quantitative prediction to which we can compare. Accordingly, we simply report the change in the excess free energy per persistence length for very long chains as a function of w/H in the inset in Figure 10. In the figure we observe that the excess free energy is small for small w, monotonically increases as the ratio w/H gets larger and saturates as w approaches the slit height.

Before leaving the subject of confined chains with excluded volume, we comment briefly on previous work that has also posited the existence of self-crossing and non-self-crossing regimes

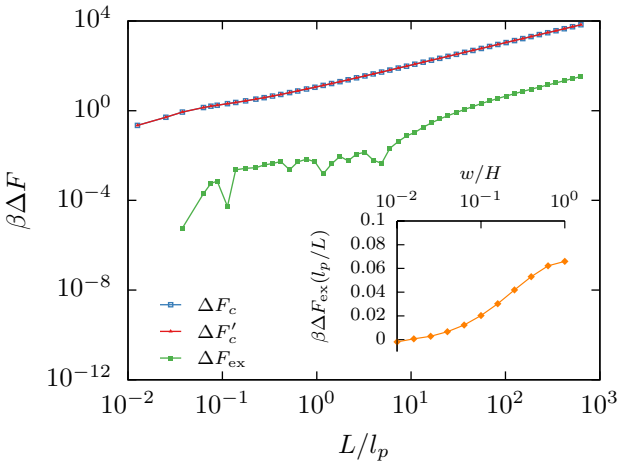

Figure 10: (main) Normalized ideal free energy of confinement, real free energy of confinement and excess free energy versus the number of persistence lengths for a chain with $H/l_p = 10^{-1.5}$ and $w/H = 0.398$. (inset) Excess free energy per persistence length for long chains ($L/a = 50001$) with a fixed value of $H/l_p = 10^{-1.5}$ and varying values of w/H. The data used for both the main panel and the inset correspond to sets 3, 5 and 7 in Table 2.

for strongly confined chains in slits.[9] As the nomenclature implies, the distinction between these possible regimes occurs when $H = 2w$; when $H < 2w$, excluded volume interactions prevent chain segments from crossing, whereas when $H \geq 2w$ no such restriction is imposed. In contrast with this idea, Figures 8 and 10 show a gradual excluded volume crossover suggested by Eq. 30 rather than a topologically constrained state. Due to these observations, we find no evidence to support the idea that a prohibition of self-crossing is responsible for the self-avoidance of strongly confined chains in slits. Furthermore, we suggest that a potential crossover at $H = 2w$ may not be universal and would be an artifact of hard beads, since softer beads could cross, depending on the choice of potential and length scale.

4 Conclusion

We have presented a comprehensive theory for the Odijk regime in nanoslits that reconciles details from both the literature on ideal chains and the literature on real chains. In particular we have shown that there are three regimes of behavior for slits where $H \ll l_p$, which we labelled the weak confinement regime, the orientational regime and the Odijk regime. Furthermore, we demonstrated

three subregimes of behavior for long chains: an Odijk-rod regime, and Odijk-Gaussian regime and an Odijk-Flory regime, the last of which only occurs for chains with excluded volume. For the Odijk regime in particular we developed a theory which describes the end-to-end distance in terms of a two-dimensional wormlike chain with out-of-plane fluctuations described by a series expansion in λ/l_p.

Numerical results are in excellent agreement with the theory. Results for the projected persistence length and confinement free energy are consistent with the three regime picture, and results for the end-to-end distance provide firm evidence for three subregimes within the Odijk regime. Additionally, we find quantitative agreement with the theory for the end-to-end distance, and using our PERM simulations we find several previously unknown prefactors for chains with excluded volume. Interestingly we find that, while conceptually important, the influence of the slit height on the end-to-end distance of an ideal chain is practically negligible. However, this is not the case for real chains, where the slit height strongly influences the excluded volume interactions of the chain.

Finally we note that this problem is quite mature in terms of theory and simulation, yet work remains to relate these rather abstract regimes to actual experimental systems. Such experiments can be quite difficult in practice, since one must use a system with a large persistence length $l_p \gg H$ and long chains $L \gg H$ relative to the slit height. Despite the difficulty, there are notable examples of recent successes in measuring semiflexible chains in the Odijk regime by Nöding and Köster[37] and by Frykholm *et al.*[38] Nevertheless, it remains to be seen if the regimes we have outlined can be observed in real systems, or whether effects such as soft or long-range potentials play a more dominant role.

Acknowledgement

This work was supported by the NSF (CBET-1262286). The authors would like to thank H.-P. Hsu, W. Paul and K. Binder for kindly providing their data for use in Figure 8. Additionally, DRT wishes to acknowledge a Doctoral Dissertation Fellowship from the University of Minnesota and many useful discussions with Abhiram Muralidhar. Computational resources were provided in part by

the University of Minnesota Supercomputing Institute.

References

(1) Jo, K.; Dhingra, D. M.; Odijk, T.; de Pablo, J. J.; Graham, M. D.; Runnheim, R.; Forrest, D.; Schwartz, D. C. *Proc. Natl. Acad. Sci. U.S.A.* **2007**, *104*, 2673–2678.

(2) Kounovsky-Shafer, K. L.; Hernández-Ortiz, J. P.; Jo, K.; Odijk, T.; de Pablo, J. J.; Schwartz, D. C. *Macromolecules* **2013**, *46*, 8356–5368.

(3) Chen, Y.-L.; Graham, M. D.; de Pablo, J. J.; Randall, G. C.; Gupta, M.; Doyle, P. S. *Phys. Rev. E* **2004**, *70*, 060901(R).

(4) Lin, P.-K.; Fu, C.; Chen, Y.; Chen, Y.; Wei, P.; Kuan, C.; Fann, W. *Phys. Rev. E* **2007**, *76*, 011806.

(5) Bonthuis, D. J.; Meyer, C.; Stein, D.; Dekker, C. *Phys. Rev. Lett.* **2008**, *101*, 108303.

(6) Odijk, T. *Phys. Rev. E* **2008**, *77*, 060901(R).

(7) Tang, J.; Levy, S. L.; Trahan, D. W.; Jones, J. J.; Craighead, H. G.; Doyle, P. S. *Macromolecules* **2010**, *43*, 7368 – 7377.

(8) Cifra, P. *J. Chem. Phys.* **2012**, *136*, 024902.

(9) Dai, L.; Jones, J. J.; van der Maarel, J. R. C.; Doyle, P. S. *Soft Matter* **2012**, *8*, 2972–2982.

(10) Strychalski, E. A.; Geist, J.; Gaitan, M.; Locascio, L. E.; Stavis, S. M. *Macromolecules* **2012**, *45*, 1602–1611.

(11) Bicout, B. J.; Burkhardt, T. W. *J. Phys. A: Math. Gen.* **2001**, *34*, 5745–5750.

(12) Yang, Y.; Burkhardt, T. W.; Gompper, G. *Phys. Rev. E* **2007**, *76*, 011804.

(13) Burkhardt, T. W.; Yang, Y.; Gompper, G. *Phys. Rev. E* **2010**, *82*, 041801.

(14) Chen, J. Z. Y.; Sullivan, D. E. *Macromolecules* **2006**, *39*, 7769–7773.

(15) Daoud, M.; de Gennes, P.-G. *J. Phys. France* **1977**, *38*, 85–93.

(16) Rivetti, C.; Guthold, M.; Bustamante, C. *J. Mol. Biol.* **1996**, *264*, 919 – 932.

(17) Hsu, H.-P.; Paul, W.; Binder, K. *Europhys. Lett.* **2011**, *95*, 68004.

(18) Grassberger, P. *Phys. Rev. E* **1997**, *56*, 3682–3693.

(19) Dorfman, K. D.; King, S. B.; Olson, D. W.; Thomas, J. D. P.; Tree, D. R. *Chem. Rev.* **2013**, *113*, 2584–2667.

(20) Odijk, T. *Macromolecules* **1983**, *16*, 1340–1344.

(21) Odijk, T. *Macromolecules* **1986**, *19*, 2313–2329.

(22) Wang, Y.; Peters, G. H.; Hansen, F. Y.; Hassager, O. *J. Chem. Phys.* **2008**, *128*, 124904.

(23) Auvray, L. *J. Phys. France* **1981**, *42*, 79–95.

(24) Muralidhar, A.; Tree, D. R.; Wang, Y.; Dorfman, K. D. *J. Chem. Phys.* **2014**, *140*, 084905.

(25) Tree, D. R.; Wang, Y.; Dorfman, K. D. *Phys. Rev. Lett.* **2013**, *110*, 208103.

(26) Casassa, E. F. *J. Polym. Sci., Part B: Polym. Lett.* **1967**, *5*, 773–778.

(27) Tree, D. R.; Muralidhar, A.; Doyle, P. S.; Dorfman, K. D. *Macromolecules* **2013**, *46*, 8369–8382.

(28) des Cloizeaux, J. *J. Phys. France* **1976**, *37*, 431–434.

(29) de Gennes, P.-G. *Scaling Concepts in Polymer Physics*; Cornell University Press, 1979.

(30) Schäfer, L. *Excluded Volume Effects in Polymer Solutions as Explained by the Renormalization Group*; Springer, 1999.

(31) Dai, L.; van der Maarel, J. R. C.; Doyle, P. S. *Macromolecules* **2014**, *In Press*.

(32) Storm, C.; Nelson, P. C. *Phys. Rev. E* **2003**, *67*, 051906.

(33) Wang, J.; Gao, H. *J. Chem. Phys.* **2005**, *123*, 084906.

(34) Wang, Y.; Tree, D. R.; Dorfman, K. D. *Macromolecules* **2011**, *44*, 6594–6604.

(35) Hsu, H.-P.; Paul, W.; Binder, K. *Macromolecules* **2010**, *43*, 3094–3102.

(36) Tree, D. R.; Wang, Y.; Dorfman, K. D. *Biomicrofluidics* **2013**, *7*, 054118.

(37) Nöding, B.; Köster, S. *Phys. Rev. Lett.* **2012**, *108*, 088101.

(38) Frykholm, K.; Alizadehheidari, M.; Fritzsche, J.; Wigenius, J.; Modesti, M.; Persson, F.; Westerlund, F. *Small* **2014**, *10*, 884–887.

For Table of Contents use only

Title: The Odijk Regime in Slits

Authors: Douglas R. Tree, Wesley F. Reinhart, and Kevin D. Dorfman*